Nuclear Engineering and Technology 53 (2021) 2251–2260

Contents lists available at ScienceDirect

Nuclear Engineering and Technology

journal homepage: www.elsevier.com/locate/net

Original Article

Fuzzy-PID controller for motion control of CFETR multi-functional maintenance platform

Dongyi Li [a, b, c], Kun Lu [a], Yong Cheng [a, c], Wenlong Zhao [a, c, *], Songzhu Yang [a, c], Yu Zhang [a, c], Junwei Li [a, b, c], Huapeng Wu [d]

[a] Institute of Plasma Physics, Hefei Institutes of Physical Science, Chinese Academy of Sciences, Hefei, China
[b] University of Science and Technology of China, Hefei, China
[c] Anhui Extreme Environment Robot Engineering Laboratory, Hefei, China
[d] Lappeenranta University of Technology, Lappeenranta, Finland

ARTICLE INFO

Article history:
Received 8 September 2020
Received in revised form
13 January 2021
Accepted 25 January 2021
Available online 3 February 2021

Keywords:
CFETR
Parallel robot
Kinematics analysis
Hydraulics
Fuzzy-PID
Simulation

ABSTRACT

The motion control of the divertor maintenance system of the China Fusion Engineering Test Reactor (CFETR) was studied in this paper, in which CFETR Multi-Functional Maintenance Platform (MFMP) was simplified as a parallel robot for the convenience of theoretical analysis. In order to design the motion controller of parallel robot, the kinematics analysis of parallel robot was carried out. After that, the dynamic modeling of the hydraulic system was built. As the large variation of heavy payload on MFMP and highly nonlinearity of the system, A Fuzzy-PID controller was built for self-tuning PID controller parameters by using Fuzzy system to achieve better performance. In order to test the feasibility of the Fuzzy-PID controller, the simulation model of the system was built in Simulink. The results have showed that Fuzzy-PID controller can significantly reduce the angular error of the moving platform and provide the stable motion for transferring the divertor.

1. Introduction

The China Fusion Engineering Test Reactor is a new Tokamak proposed by China to lay the foundation for the establishment of the China's commercial fusion reactors in the future. As an important component of the CFETR, the divertor needs to be maintained by the Multi-Function Maintenance Platform (Fig. 1). The moving platform of MFMP is controlled by the oil highly airtight hydraulic cylinders. The requirement of the position accuracy of the moving platform is 10% of the whole stroke. In order to transfer the divertor smoothly, the position of the moving platform of the MFMP is needed to control precisely, and this is the focus of this article.

With the simplified design, the moving platform can be regarded as a 3-RPS parallel robot as shown in Fig. 2 [1]. The motion control methods of parallel robot can be divided into two categories: motion control in motion space and joint space [2–4]. Compared with the motion control in motion space, the motion control in joint space is easier to implement in practice. Based on the parameters of each joint and the reverse kinematics model of parallel robot, the expected joint data $\boldsymbol{q}_d$ is calculated according to the expected trajectory $\boldsymbol{\chi}_d$ of the robot, and the motion error $\boldsymbol{e}_q$ in the joint space is obtained by measuring the driving joints' data $\boldsymbol{q}$ (Fig. 3).

Although the traditional PID control method is widely used in engineering, it had limitations. In order to achieve better control, the PID control parameters need to be modified in real time according to the actual control situation. The Fuzzy control is based on the fuzzy set theory and fuzzy logic inference. The fuzzy reasoning mechanism is based on the expert knowledge and the operator's actual experience, and is accurate to some extent and has the characteristics of autonomous learning in application. The fuzzy control does not need accurate mathematical model of the system, and it is suitable for complex nonlinear control system [5,6]. Therefore, an incremental PID control method based on the fuzzy control to reduce the control error and improve the control accuracy by adjusting the values of K_p, K_i and K_d during the system operation was studied [7–15].

* Corresponding author. Institute of Plasma Physics, Hefei Institutes of Physical Science, Chinese Academy of Sciences, Hefei, China.
E-mail address: zhwl@ipp.ac.cn (W. Zhao).

https://doi.org/10.1016/j.net.2021.01.025

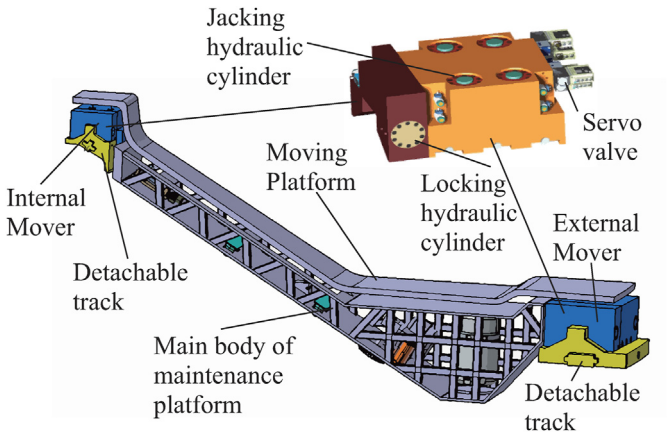

Fig. 1. Diagram of divertor MFMP.

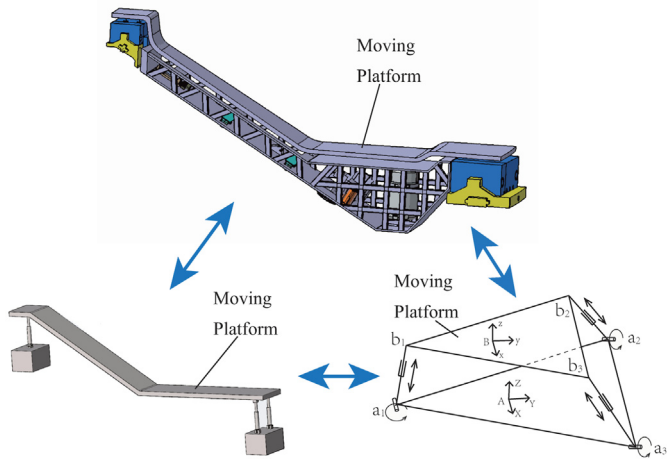

Fig. 2. Simplification process of moving platform of MFMP.

2. Kinematics analysis of 3-RPS parallel robot

2.1. Inverse kinematics

In order to solve the length $L = [l_1, l_2, l_3]^T$ of each drive rod, the closed loop equation of each branch chain is written as:

$$l_i \overset{A}{\hat{\boldsymbol{s}}}_i = {}^A\boldsymbol{P} + {}^A\boldsymbol{b}_i - {}^A\boldsymbol{a}_i = {}^A\boldsymbol{P} + {}^A\boldsymbol{R}_B{}^B\boldsymbol{b}_i - {}^A\boldsymbol{a}_i \tag{1}$$

where,

$i = 1, 2, 3$;

$\hat{\boldsymbol{s}}_i$——Unit vector from point a_i in fixed platform to point b_i in moving platform;

${}^A\boldsymbol{P}$——The position vector of the moving platform center point B in the reference coordinate system {A} (Fig. 4) [1];

${}^A\boldsymbol{a}_i$——The position vector of joint points a_i on fixed platform respect to the reference coordinate system {A};

${}^A\boldsymbol{b}_i$——The position vector of joint points b_i on the moving platform respect to the reference coordinate system {A};

${}^A\boldsymbol{R}_B$——The rotation matrix of the moving coordinate system {B} relative to the reference coordinate system {A}.

From Eq. (1), we can obtain this:

$$l_i = \left[{}^A\boldsymbol{P}^T{}^A\boldsymbol{P} + {}^B\boldsymbol{b}_i^T{}^B\boldsymbol{b}_i + {}^A\boldsymbol{a}_i^T{}^A\boldsymbol{a}_i - 2{}^A\boldsymbol{P}^T{}^A\boldsymbol{a}_i + 2{}^A\boldsymbol{P}^T\left[{}^A\boldsymbol{R}_B{}^B\boldsymbol{b}_i\right] - 2\left[{}^A\boldsymbol{R}_B{}^B\boldsymbol{b}_i\right]^T{}^A\boldsymbol{a}_i \right]^{1/2} \tag{2}$$

2.2. Forward kinematics

Given the length of each branch chain $L = [l_1, l_2, l_3]^T$, we can obtain the position vector ${}^A\boldsymbol{P} = [p_x, p_y, p_z]^T$ and the rotation angle parameters of the moving platform $\theta = [\alpha, \beta, \gamma]^T$.

Numerical solutions can be obtained by the following nonlinear equations using nonlinear least squares method ($F({}^A\boldsymbol{P}, \theta) = 0$).

$$\begin{cases} F_i\left({}^A\boldsymbol{P}, \theta\right) = -l_i^2 + \left[{}^A\boldsymbol{P} + {}^A\boldsymbol{R}_B{}^B\boldsymbol{b}_i - {}^A\boldsymbol{a}_i\right]^T\left[{}^A\boldsymbol{P} + {}^A\boldsymbol{R}_B{}^B\boldsymbol{b}_i - {}^A\boldsymbol{a}_i\right] \\ F_4\left({}^A\boldsymbol{P}, \theta\right) = p_x \\ F_5\left({}^A\boldsymbol{P}, \theta\right) = p_y \\ F_6\left({}^A\boldsymbol{P}, \theta\right) = \alpha \end{cases}$$

where, $i = 1, 2, 3$.

3. Hydraulic system model

As the models of hydraulic components are nonlinear, in order to simplify the analysis, the zero-opening four-way slide valve was adopted to control the hydraulic cylinder (Fig. 5), the nonlinear equations were linearized [16–18]. The following assumptions were given: (1) the valve is an ideal zero-opening slide valve, and the hydraulic cylinder is symmetrical; (2) the pump pressure is constant.

3.1. Electromagnetic valve model

The response of spool of the electromagnetic valve to the input voltage can be described as a first-order transfer function:

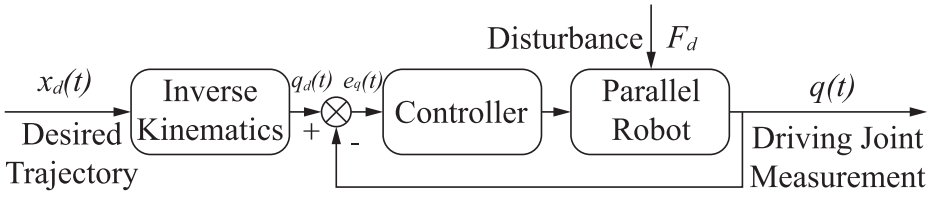

Fig. 3. Motion control in joint space.

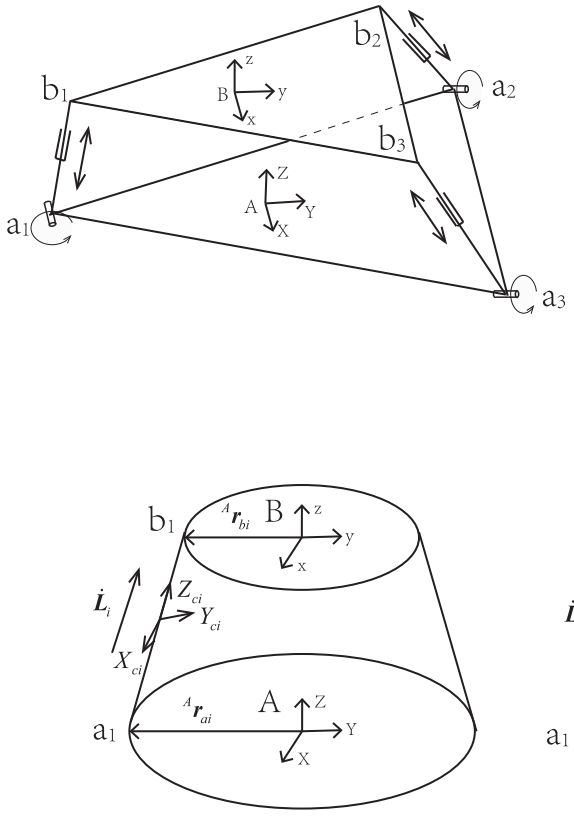

Fig. 4. Diagram of parameters of parallel mechanism.

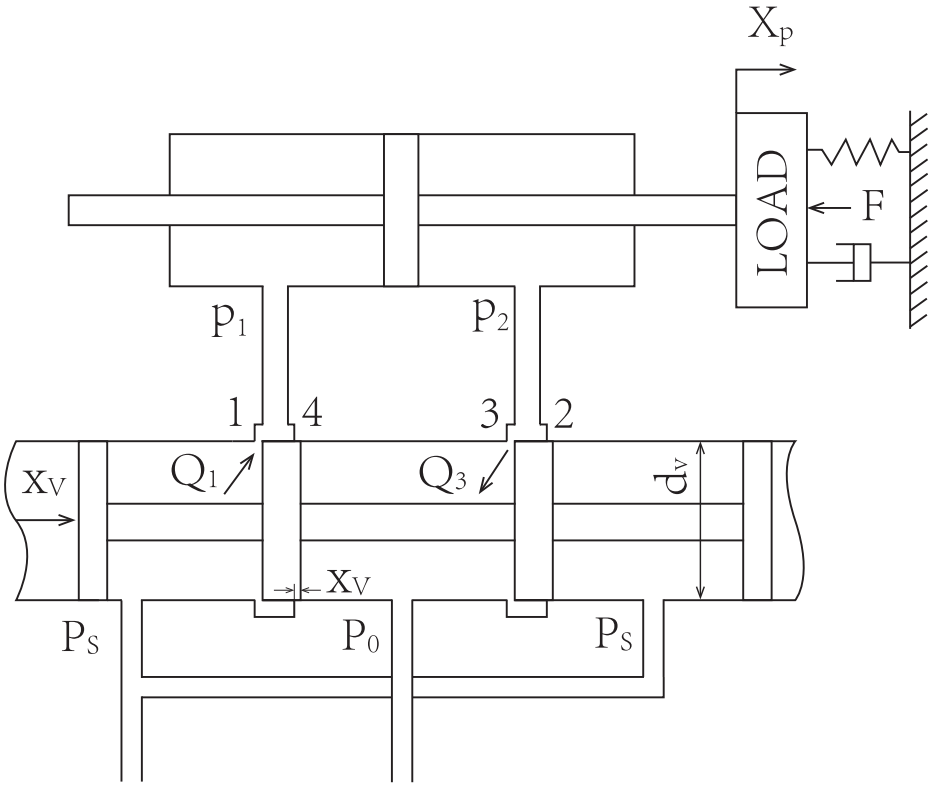

Fig. 5. Schematic diagram of symmetrical hydraulic cylinder controlled by electromagnetic valve.

$$G(s) = \frac{\boldsymbol{X_v}}{\boldsymbol{U_i}} = \frac{k_v}{1 + \tau_v s} \tag{3}$$

where,

X_v——The spool displacement;
u_i——The input voltage signal;
τ_v——The time constant, which can be measured through the frequency response of the valve;
k_v——The gain.

3.2. Mathematical model of servo hydraulic cylinder system

3.2.1. Linearized flow equation

Let the value of x_v (Fig. 5) be positive, Eqs. (4) and (5) represent the flow at orifices 1 and 3 respectively.

$$Q_1 = C_d \omega x_v \sqrt{\frac{2}{\rho}(P_s - P_1)} \tag{4}$$

$$Q_3 = C_d \omega x_v \sqrt{\frac{2}{\rho}(P_2 - P_0)} \tag{5}$$

$$P_L = P_1 - P_2 \tag{6}$$

where,

ω——The perimeter of the orifice;
P_0——Return pressure, usually, $P_0 \approx 0$;
P_L——The load pressure.

Under the ideal conditions:

$$Q_1 = Q_3 = Q_L \tag{7}$$

That is:

$$P_s = P_1 + P_2 \tag{8}$$

From Eqs. (4), (6) and (8), we obtained:

$$Q_L = C_d \omega x_v \sqrt{\frac{1}{\rho}(P_s - P_L)} \tag{9}$$

Eq. (9) is a nonlinear equation representing the flow rate of the servo hydraulic cylinder, but the right hand side of the equation can be linearized by a Tylor series expansion, using only the first two terms:

$$\Delta Q_L = \frac{\partial Q_L}{\partial x_v}\Delta x_v + \frac{\partial Q_L}{\partial P_L}\Delta P_L \tag{10}$$

Or:

$$\Delta Q_L = K_q \Delta x_v - K_c \Delta P_L \tag{11}$$

where,

K_q——The flow gain, which is the flow increment caused by small displacement of spool when load pressure is constant;
K_c——The pressure flow coefficient, which represents the relationship between the load pressure increment and the load flow when the spool displacement is constant.

Since the system is usually at zero point, i.e., $Q_L = x_v = P_L = 0$, the coefficient of the valve at zero point is obtained as following:

$$K_{q0} = C_d \omega \sqrt{\frac{1}{\rho} P_s} \tag{12}$$

$$K_{c0} = 0 \tag{13}$$

Since the initial state of the zero-opening valve was set at zero, increments $\Delta Q_L = Q_L$, $\Delta x_v = x_v$, $\Delta P_L = P_L$, and Eq. (11) can be written as follows:

$$Q_L = K_{q0} x_v - K_{c0} P_L \tag{14}$$

3.2.2. Flow rate continuation equation

In the actual situation, $Q_1 \neq Q_3 \neq Q_L$ due to the oil compression, the gap leakage and other factors, and now the load flow Q_L is redefined as follow:

$$Q_L = \frac{1}{2}(Q_1 + Q_3) \tag{15}$$

Definition:

$$\Delta P = \beta_e \frac{\Delta V}{V} \tag{16}$$

That is:

$$Q = \frac{dV}{dt} = \frac{V}{\beta_e}\frac{dP}{dt} \tag{17}$$

where,

ΔP——The increment of pressure in the container;
ΔV——The liquid compression;
V——The initial volume of the liquid in the container;
β_e——The liquid equivalent volume modulus of elasticity.

Considering that the liquid flowing into the hydraulic cylinder will be affected by compression, leakage and other factors, the flow rate into the left chamber of the hydraulic cylinder piston is obtained:

$$Q_1 = A_p \frac{dx_p}{dt} + \frac{V_1}{\beta_e}\frac{dP_1}{dt} + C_i(P_1 - P_2) + C_e P_1 \tag{18}$$

where,

A_p——The piston area;
x_p——The piston displacement;
P_1——The pressure of the piston's left hand chamber;
V_1——The total volume of liquid at pressure P_1;
C_i——The coefficient of internal leakage;
C_e——The coefficient of external leakage.

The following formula is obtained in the same way:

$$Q_3 = A_p \frac{dx_p}{dt} - \frac{V_2}{\beta_e}\frac{dP_2}{dt} + C_i(P_1 - P_2) - C_e P_2 \tag{19}$$

where,

V_2——The total volume of liquid at pressure P_2;
P_2——The pressure of the piston's right hand chamber.

Based on Eqs. (15), (18) and (19), the flow continuation equation is obtained:

$$Q_L = A_p\frac{dx_p}{dt} + \frac{V_t}{4\beta_e}\frac{dP_L}{dt} + C_tP_L \tag{20}$$

where,

V_t——The equivalent gross volume of hydraulic cylinder, $V_t = V_1 + V_2$;
C_t——The total leakage coefficient, $C_t = C_i + \frac{C_e}{2}$.

3.2.3. Force equilibrium equation

The thrust generated by the hydraulic cylinder is balanced with the inertia force, the viscous friction force, the elastic load force and the external load. It can be written as follows:

$$A_pP_L = M\frac{d^2x_p}{dt^2} + B\frac{dx_p}{dt} + kx_p + F_L \tag{21}$$

where,

M——The piston mass and the total mass converted from the load to the piston;
B——The coefficient of viscous friction of piston and load;
k——The elastic load stiffness;
F_L——Other loads acting on the piston.

3.2.4. Transfer function

By applying the Laplace Transformation to Eqs. (14), (20) and (21), the following equations can be obtained:

$$\boldsymbol{Q_L} = K_{q0}\boldsymbol{X_v} - K_{c0}\boldsymbol{P_L} \tag{22}$$

$$\boldsymbol{Q_L} = A_p s\boldsymbol{X_p} + \frac{V_t}{4\beta_e}s\boldsymbol{P_L} + C_t\boldsymbol{P_L} \tag{23}$$

$$A_p\boldsymbol{P_L} = Ms^2\boldsymbol{X_p} + Bs\boldsymbol{X_p} + k\boldsymbol{X_p} + \boldsymbol{F_L} \tag{24}$$

From Eqs. (22)–(24), the transfer function is obtained:

$$\boldsymbol{X_p} = \frac{\frac{K_{q0}}{A_p}\boldsymbol{X_v} - \frac{K_{ce}}{A_p^2}\left(\frac{V_t}{4\beta_eK_{ce}}s + 1\right)\boldsymbol{F_L}}{\frac{V_tM}{4\beta_eA_p^2}s^3 + \left(\frac{K_{ce}M}{A_p^2} + \frac{V_tB}{4\beta_eA_p^2}\right)s^2 + \left(\frac{V_tk}{4\beta_eA_p^2} + \frac{K_{ce}B}{A_p^2} + 1\right)s + \frac{K_{ce}k}{A_p^2}} \tag{25}$$

$$\boldsymbol{U_o} = k_g\boldsymbol{X_p} \tag{26}$$

where,

U_o——The output voltage signal;
K_{ce}——The total pressure flow coefficient, $K_{ce} = K_{c0} + C_t$;
k_g——The displacement-pressure conversion coefficient

By combining Eqs. (3), (25) and (26), the relationship between the input $\boldsymbol{U_i}$ and the output $\boldsymbol{U_o}$ is obtained. After obtaining the transfer function of $U_i - X_p$, a PID controller can be applied to a position control system.

$$u(t) = k_pe(t) + k_i\int_0^t e(t)dt + k_d\frac{de(t)}{dt} \tag{27}$$

where,

$u(t)$——The output of controller;
$e(t)$——The error in control system;
k_p, k_i *and* k_d——The PID parameters.

From Eq. (27), proportion part decreases system errors proportionally; integration part decreases the system cumulative errors; differentiation part represents the change ratio of system error and speeds up the decrease of the system errors.

4. Fuzzy-PID controller design

4.1. Tuning PID parameters

After the transfer function of the servo-valve controlled hydraulic cylinder is obtained, the parameters of the PID controller can be adjusted through the transfer function, (Fig. 6). The parameters' setting in the hydraulic system is shown in Table 1.

The parameters of the PID controller can also be obtained by using the PID Tuner application of MATLAB (Fig. 7). After serval experimental adjustments in PID Tuner, the optimal PID parameters were found. Then, these PID parameters are set as the initial PID parameters K_{p0}, K_{i0} *and* K_{d0} in the Fuzzy-PID controller.

4.2. Fuzzy-PID controller design

In this article, a two-dimensional fuzzy controller was adopted, having its input variables as error E and the error variation Ec and its output variables as ΔK_p, ΔK_i and ΔK_d. All variables in this system were classified into seven fuzzy subsets, and the corresponding language values of the Fuzzy method is $\{PB, PM, PS, Z, NS, NM, NB\}$. The fuzzy field of E and ΔK_p is [-6,6]; The fuzzy field of Ec, ΔK_i and ΔK_d is [-3,3]. In this work, the membership functions of E and Ec were selected as the Gaussian type; the membership functions of ΔK_p, ΔK_i and ΔK_d were selected as the triangular type; and the fuzzy rules were determined based on the technical knowledge and operation experience of technicians. Finally, with the Fuzzy module of MATLAB, the output of the Fuzzy controller (ΔK_p, ΔK_i and ΔK_d) is obtained.

$$K_p = K_{p0} + \Delta K_p \tag{28}$$

$$K_i = K_{i0} + \Delta K_i \tag{29}$$

$$K_d = K_{d0} + \Delta K_d \tag{30}$$

By combining the fuzzy control and PID control, the incremental PID controller was built (Fig. 8 and Eqs. (28)–(30)). ΔK_p, ΔK_i and ΔK_d can be gained from the Fuzzy controller. Moreover, ΔK_p, ΔK_i and ΔK_d can also be adjusted by altering their respective gains.

5. Hydraulic system simulation in simulink

5.1. The parameters of simulation

According to the actual situation, the key hydraulic system parameters were shown in Table 2. With the parameters shown in Ref. [1] and Table 3, the actual length parameters of hydraulic cylinders were calculated through the inverse kinematics in Section

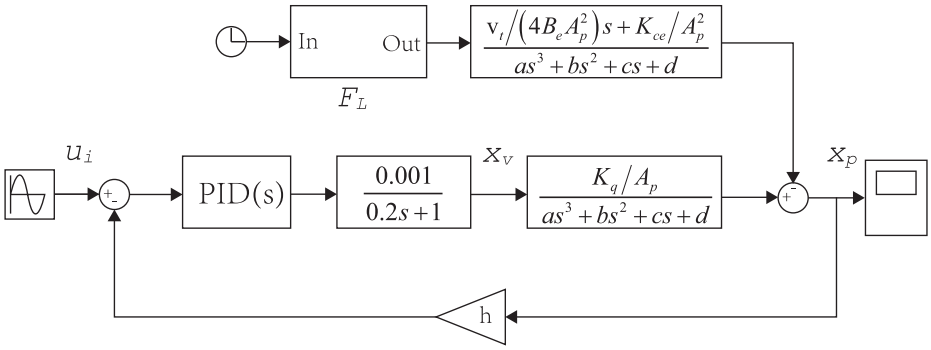

Fig. 6. PID controller in hydraulic system.

Table 1
Parameters' setting in hydraulic system.

Parameters	Values	Units
A_p	1.256×10^{-3}	m^3
C_i	5×10^{-13}	$m^5/(N \cdot S)$
C_p	0	$m^5/(N \cdot S)$
K_{c0}	0	$m^3/(S \cdot Pa)$
C_d	0.61	
M	227.7	K_g
B	628	
k	0	N/M
β_e	7×10^8	Pa
P_s	1.4×10^7	Pa
ρ	880	Kg/m^3
ω	0.157	m
τ	0.02	

2.1, and the input signal of each hydraulic cylinder was set and shown in Fig. 9. The load disturbances F_{L1}, F_{L2} and F_{L3} were obtained through the dynamic analysis of parallel robot [1], and the force distribution was carried out according to the actual number of hydraulic cylinders (Fig. 10). And the forward kinematics equations of the parallel robot in Section 2.2 was used to solve the position and pose parameters (X and Y axes angle) of the moving platform in MATLAB.

5.2. Simulation and results analysis

The simulation block diagram [19–23] was established in Simulink (Fig. 11). After the simulation, it was found that each of the PID parameters was stabilized around a certain value. Then, we changed the initial parameters according to the stabilized values of K_p, K_i and K_d. After several adjustments, the appropriate initial parameters were found.

Finally, the comparison between the designed angles in different axes (i.e., the X- and Y axis) and the actual angles under the PID control were shown in Fig. 12. Similarly, the comparison between the designed angles in the X- and Y-axis and the real angles under Fuzzy-PID control were shown in Fig. 13. The angular errors in the X-axis and the Y-axis by the two control methods were shown in Fig. 14.

It can be seen from the simulation results that the maximum angular error of rotation around the X-axis reached 7.115% of the maximum stroke; while the maximum angular error of rotation about the Y-axis reached 5.893% of the maximum stroke. The maximum angular error of the moving platform around the X-axis was about 1.5514×10^{-3}°, reaching 2.221% of the maximum stroke; while the maximum angular error of the moving platform around the Y-axis was about 1.5514×10^{-3}°, reaching 2.586% of the maximum stroke.

By comparing the performances of the PID controller and the Fuzzy-PID controller, it is clear that the Fuzzy-PID controller

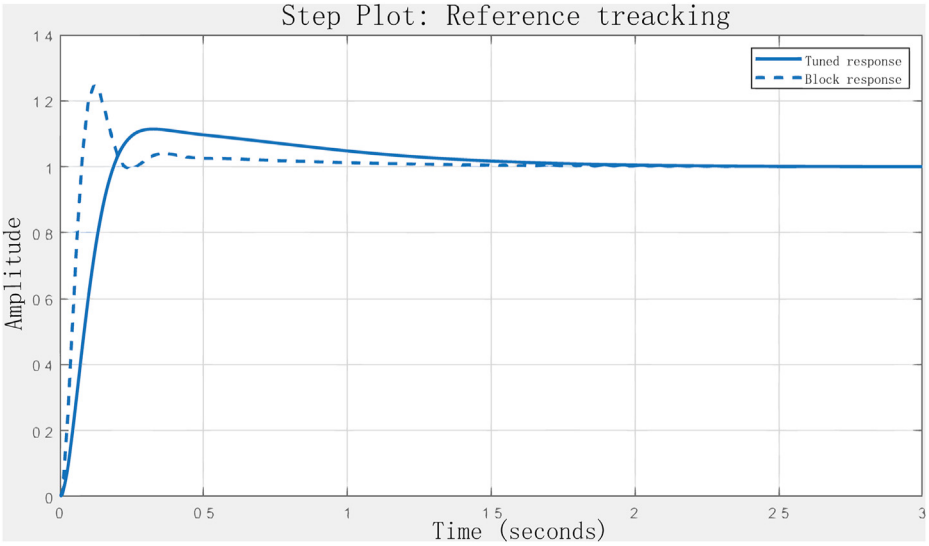

Fig. 7. Tuning PID parameter in PID tuner (The dash line is for the original response and the solid line for the tuned response).

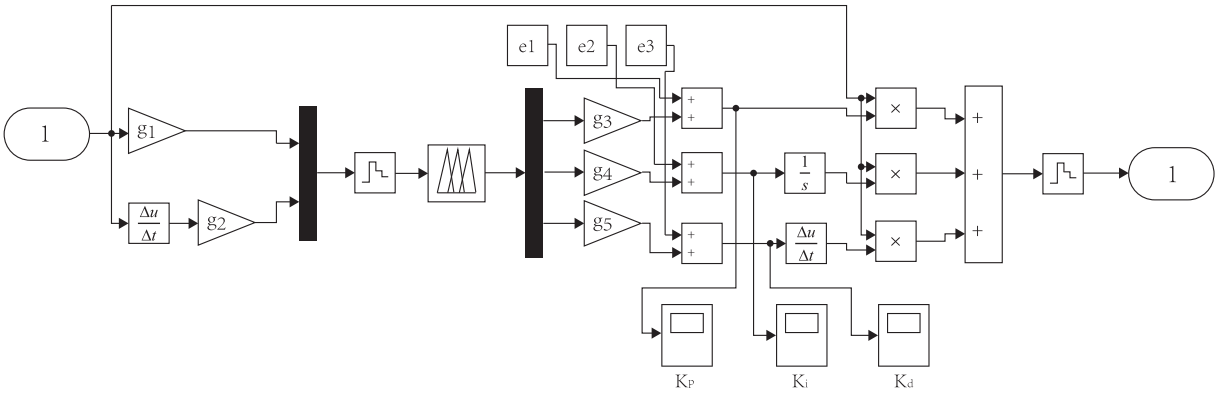

Fig. 8. Fuzzy-PID controller.

Table 2
The key parameters of hydraulic system.

Parameters	Values	Units
Hydraulic cylinder stroke	0.15	m
Hydraulic cylinder internal diameter	50	mm
Diameter of piston rod	30	mm
Servo valve natural frequency	50	Hz
Pump flow	35	L/min
Rated Load	15	ton
Seismic load	3	level

Table 3
The trajectory of the moving platform.

Coordinates	Value
x/ m	0
y/ m	0
z/ m	0.516
α/ rad	0
β/ rad	$0.03\sin(t+\pi/2)$
γ/ rad	$0.03\cos(t+\pi/2)$

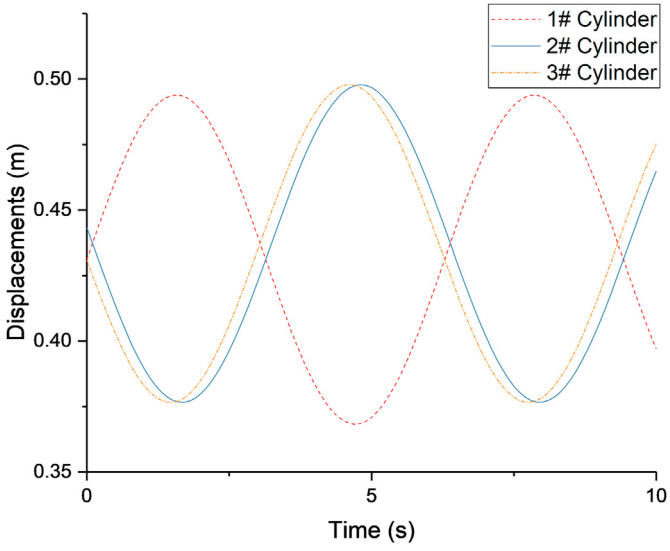

Fig. 9. Hydraulic cylinder displacement input signal.

reduced the angular error of rotation around the X-axis and Y-axis by approximately half.

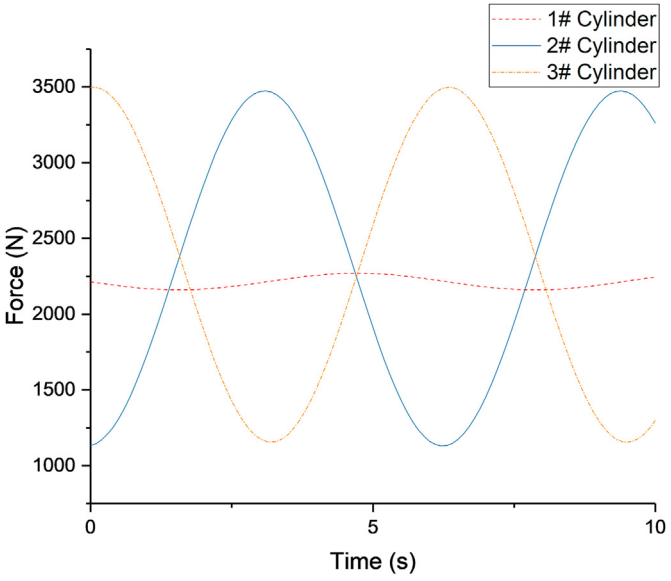

Fig. 10. Loads for hydraulic cylinders.

6. Conclusion

In this work, Fuzzy-PID algorithm was used to control the motion of the divertor MFMP moving platform. Firstly, the transfer function of the servo valve and hydraulic cylinder was built. Based on the transfer function, the initial PID parameters that meet the stability and accuracy were found. Because the parameters of the PID controller were fixed, the angular error cannot be eliminated in real time after the external force F_L was added, yet the error did not converge. In order to reduce the error, the Fuzzy-PID controller was built. By the errors and values of parameters of all PID controllers, the parameters of the PID controllers were modified repeatedly. After serval adjustments, the appropriate parameters for the Fuzzy-PID controller were found. Because the fuzzy control can adjust parameters in real time, the control error will not be affected by F_L after adding the external force. Finally, the good control effect has been obtained, and the achieved results have indicated that the Fuzzy-PID controller is relatively more stable and accurate in the maintenance of the divertor.

The fuzzy-PID control method will be adapted in the synchronization control of divertor MFMP in the future work.

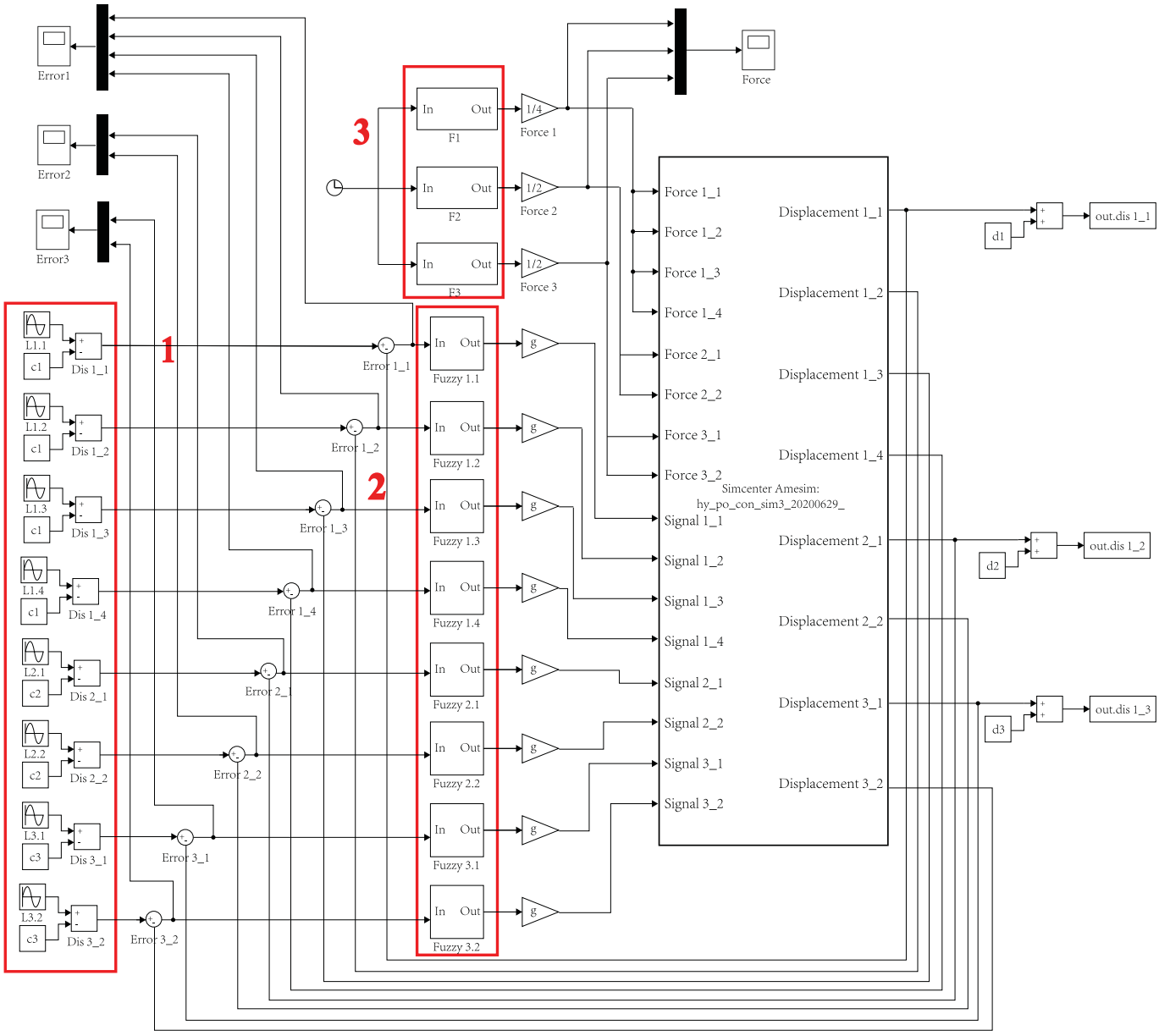

Fig. 11. Simulation diagram in Simulink
1-Displacement signal input 2-Fuzzy-PID controller 3-Force input.

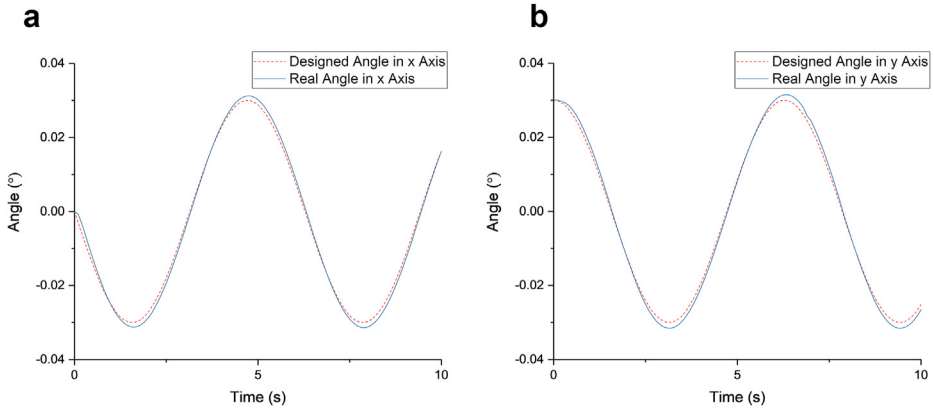

Fig. 12. Comparison rotation angle in PID controller.

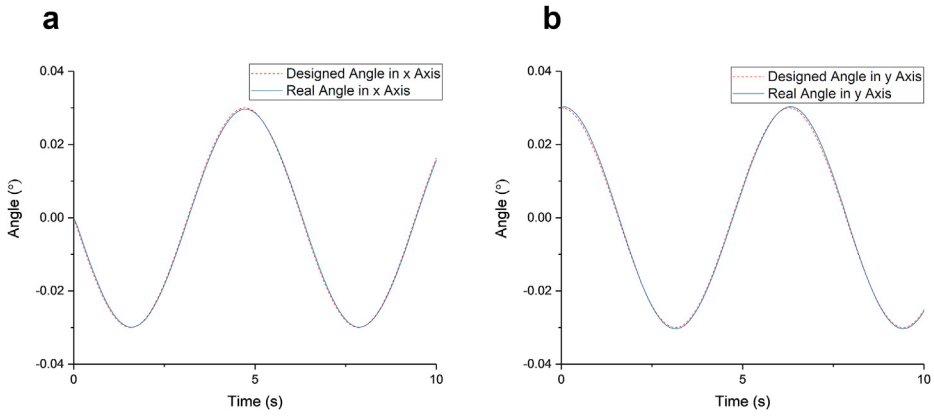

Fig. 13. Comparison of rotation angle in Fuzzy-PID controller.

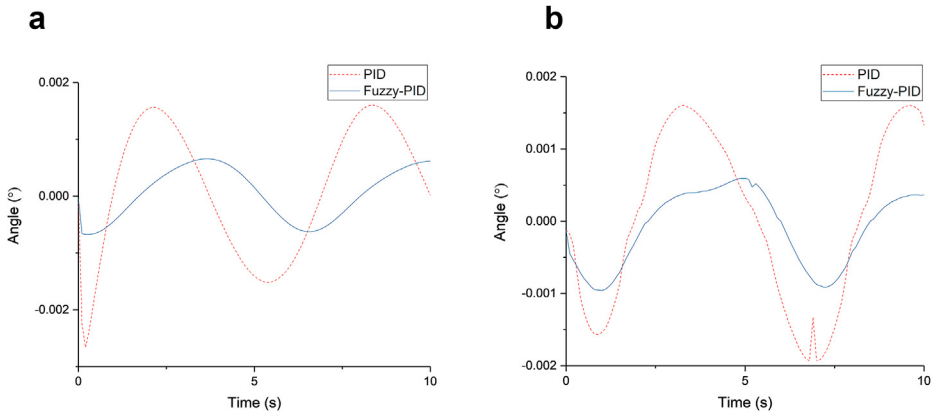

Fig. 14. Angle error comparison under different control methods.

Declaration of competing interest

The authors declare that they have no known competing financial interests or personal relationships that could have appeared to influence the work reported in this paper.

Acknowledgement

This work is supported by the National Key R&D Program of China with Grant No. 2017YFE0300503 , Comprehensive Research Facility for Fusion Technology Program of China under Contract No. 2018-000052-73-01-001228 and Anhui Extreme Environment Robot Engineering Laboratory. The authors would like to express their sincere gratitude to all the members of CFETR engineering design team.

Appendix A. Supplementary data

Supplementary data to this article can be found online at https://doi.org/10.1016/j.net.2021.01.025.

References

[1] D. Li, K. Lu, Y. Cheng, W. Zhao, S. Yang, Y. Zhang, J. Li, S. Shi, Dynamic analysis of multi-functional maintenance platform based on Newton-Euler method and improved virtual work principle, Nuclear Engineering and Technology 52 (2020) 2630–2637.
[2] H.D. Taghirad, Parallel Robots: Mechanics and Control, first ed., CRC, Boca, Raton, 2013.
[3] S. Staicu, Dynamics of Parallel Robots, first ed., Springer, Cham, Switzerland, 2019.
[4] B. Siciliano, O. Khatib, Springer Handbook of Robotics, first ed., Springer, Heidelberg, Berlin, 2008.
[5] Wenliang Deng, Baomin Qiang, Simulation of Fuzzy-PID control of dual cylinder synchronous hydraulic system, Machine Tool & Hydraulics 38 (2010) 28–30.
[6] J. Anzurez, L.A. Torres, I.I. Lazaro, Fuzzy logic control for a two tanks hydraulic system model, in: IEEE Electronics, Robotics & Automotive Mechanics Conference, Cuernavaca, Mexico, November 15-18, 2011.
[7] Y. Jing, C. Xiaoming, Z. Yang, Y. Li, Cross-coupled fuzzy PID control combined with full decoupling compensation method for double cylinder servo control system, J. Mech. Sci. Technol. 32 (2018) 2261–2271.
[8] L. Zhixing, K. Xing, Application of fuzzy PID controller for electro-hydraulic servo position control system, in: 2017 3rd IEEE International Conference on Control Science and Systems Engineering, Beijing, China, August 17-19, 2017.
[9] S. Qian, L. Hak-Keung, X. Chengbin, M. Chen, Adaptive neuro-fuzzy PID controller based on twin delayed deep deterministic policy gradient algorithm, Neurocomputing 402 (2020) 183–194.
[10] J. Xin, C. Kaikang, Z. Yang, J. Jiangtao, P. Jing, Simulation of hydraulic transplanting robot control system based on fuzzy PID controller, Measurement 164 (2020) 108023.
[11] B. Wafa, Y. AbuRmaileh, Decentralized motion control for omnidirectional wheelchair tracking error elimination using PD-fuzzy-P and GA-PID controllers, Sensors 20 (2020) 3525.
[12] C.B. Jabeur, H. Seddik, Design of a PID optimized neural networks and PD fuzzy logic controllers for a two-wheeled mobile robot, Asian J. Contr. 23 (1) (2020) 23–41.
[13] S. Bongsub, P. Jongwon, D. Yun, Depth-adaptive controller for spent nuclear fuel inspections, Nuclear Engineering and Technology 52 (2020) 1669–1676.
[14] S. Hocheol, J. Seung Ho, C. You Rack, C. Kim, Development of a shared remote control robot for aerial work in nuclear power plants, Nuclear Engineering and Technology 50 (2018) 613–618.
[15] K. Jong Seog, Y.H. Jang, Development of stable walking robot for accident condition monitoring on uneven floors in a nuclear power plant, Nuclear Engineering and Technology 49 (2017) 632–637.
[16] W. Sun, Hydraulic Control System, first ed., National defence industry press, Beijing, China, 1985.

[17] L. Zhang, Design and Use of Hydraulic Control System, first ed., Chemical Industry Press, Beijing, China, 2013.
[18] J. Lu, Automatic Control Theory, second ed., Northwestern Polytechnical University Press, Xi'an, China, 2009.
[19] Q. Liang, Q. Su, AMESim Computer Simulation Guide for Hydraulic System, first ed., China Machine Press, Bejing, China, 2014.
[20] X. Xu, Z.X. Li, H.L. Qin, Design and integrated simulation of the electro-hydraulic servo system based on AMESim and matlab, Appl. Mech. Mater. 44–47 (2011) 1355–1359.
[21] Q. Guodong, J. Aihong, C. Yong, Z. Wenlong, P. Hongtao, S. Shanshuang, Y. Song, Design and analysis of the hydraulic driving system for the circular transfer platform of the CFETR divertor, Fusion Eng. Des. 156 (2020) 111598.
[22] X.U. Bao-Qiang, W.U. Yong, Y. Wang, L.P. Zhan, Modeling and simulation of hydraulic cylinder position control based on AMESim, Coal Mine Machinery 36 (2015) 113–115.
[23] B. Wang, R.P. Xiong, Y.W. Zhao, Y. Deng, C.Y. Cheng, S.H. Shu, Research on pressure control of dual-pump direct-drive electro-hydraulic servo system based on AMESim-MATLAB joint simulation, Chin. Hydraul. Pneum. (2020) 171–176, 01.